Renner–Teller intersections along the collinear axes of polyatomic molecules: H 2 CN as a case study

Anita Das, Debasis Mukhopadhyay, Satrajit Adhikari, and Michael Baer

Citation: The Journal of Chemical Physics **133**, 084107 (2010); doi: 10.1063/1.3479399
View online: http://dx.doi.org/10.1063/1.3479399
View Table of Contents: http://scitation.aip.org/content/aip/journal/jcp/133/8?ver=pdfcov
Published by the AIP Publishing

Renner–Teller intersections along the collinear axes of polyatomic molecules: H_2CN as a case study

Anita Das,[1] Debasis Mukhopadhyay,[1,a)] Satrajit Adhikari,[2] and Michael Baer[3,b)]
[1]*Department of Chemistry, University of Calcutta, Kolkata 700 009, India*
[2]*Department of Physical Chemistry, Indian Association for Cultivation of Science, Jadavpur, Kolkata 700 032, India*
[3]*The Fritz Haber Research Center for Molecular Dynamics, The Hebrew University of Jerusalem, Jerusalem 91904, Israel*

(Received 20 April 2010; accepted 26 July 2010; published online 31 August 2010)

The tetra-atomic $C_2H_2^+$ cation is known to form Renner–Teller-type intersections along its collinear axis. Not too long ago, we studied the nonadiabatic coupling terms (NACTs) of this molecule [G. J. Halász *et al.*, J. Chem. Phys. **126**, 154309 (2007)] and revealed two kinds of intersections. (i) By employing one of the hydrogens as a test particle, we revealed the fact that indeed the corresponding (angular) NACTs produce topological (Berry) phases that are equal to 2π, which is a result anticipated in the case of Renner–Teller intersections. (ii) However, to our big surprise, repeating this study when one of the atoms (in this case a hydrogen) is shifted from the collinear arrangement yields for the corresponding topological phase a value that equals π (and not 2π). In other words, shifting (even slightly) one of the atoms from the collinear arrangement causes the intersection to change its character and become a Jahn–Teller intersection. This somewhat unexpected novel result was later further analyzed and confirmed by other groups [e.g., T. Vertesi and R. Englman, J. Phys. B **41**, 025102 (2008)]. The present article is devoted to another tetra-atomic molecule, namely, the H_2CN molecule, which just like the $C_2H_2^+$ ion, is characterized by Renner–Teller intersections along its collinear axis. Indeed, we revealed the existence of Renner–Teller intersections along the collinear axis, but in contrast to the $C_2H_2^+$ case a shift of one atom from the collinear arrangement did not form Jahn–Teller intersections. What we found instead is that the noncollinear molecule was not affected by the shift and kept its Renner–Teller character. Another issue treated in this article is the extension of (the two-state) Berry (topological) phase to situations with numerous strongly interacting states. So far the relevance of the Berry phase was tested for systems characterized by two *isolated* interacting states, although it is defined for any number of interacting states [M. V. Berry, Proc. R. Soc. London, Ser. A **392**, 45 (1984)]. We intend to show how to overcome this limitation and get a valid, fully justified definition of a Berry phase for an isolated system of any number of interacting states (as is expected). © *2010 American Institute of Physics*. [doi:10.1063/1.3479399]

I. INTRODUCTION

In a recent series of studies of tri- and tetra-atomic molecules, we considered the Renner–Teller (RT) effect as a topological phenomenon caused by degeneracy points located along the collinear axis of the studied molecule. As a first example, we chose the triatomic molecule, NH_2 (Ref. 1), and for the second example, we chose the tetra-atomic cation, $C_2H_2^+$.[2] In both cases, the degeneracy is formed along this axis by the two Π-states $1\,^2A''$ and $1\,^2A'$.[3–8] According to the Jahn–Teller (JT) terminology, such a line of degeneracy points is called a *seam* and the topological phenomenon is revealed by employing closed contours, Γ, which surround these seams.[9] To be more specific, just like in the study of the JT effect,[9,10] one of the atoms is allowed to surround the assumed seam (in this case, the axis of the collinear molecule), and while doing that, we calculate the corresponding electronic nonadiabatic coupling terms (NACTs) and then the adiabatic-to-diabatic transformation (ADT) angles, as well as the topological phases (also known as the Berry phases) or the diagonal elements of the topological **D**-matrix elements (in case the manifold contains more than two states[9]). All these facts are assumed to be known to the reader and will be elaborated here only briefly. Also, justifications for doing these studies were given on numerous occasions[1,2,9,10] and therefore are omitted in the present article.

The two abovementioned kinds of intersections differ from each other mainly because of the type of states that are involved in forming the corresponding NACTs while being in *distorted configurations*. The JT NACTs are in most cases (see next section) formed by states of the *same* symmetry such as two A' states, namely, $1\,^2A'$ and $2\,^2A'$ belonging to two different electronic states,[10(a),11,12] whereas the RT NACTs are formed by states of *different* symmetry, e.g., A' and A'' states.[3–8] These facts have implications regarding the geometrical location of the seams in configuration space and

a)Author to whom correspondence should be addressed. Electronic mail: dm_chem_cu@yahoo.in.
b)Electronic mail: michaelb@fh.huji.ac.il.

in the resulting topological features. The JT intersections were studied for numerous systems and as far as we can tell the seams are *accidental*, namely, in *most* cases they are not associated with any particular geometrical feature of the molecular system.[9,10] It is true that there are *exceptions*, for instance, the triatomic molecules X_3 for which degeneracy points are encountered at the equilateral points and the *seams* are the lines that connect these points (while varying the interatomic distance).[13]

At this stage, the following comment has to be made: Three decades ago, these *exceptions* were considered to be the *generic* JT cases [13(a)] and only more recent numerical studies showed that they are, indeed, rare.[9,10,14,25] It is important to emphasize that the generic (in contrast to the accidental) JT intersections are formed by states of *different* symmetry.

In addition, we find that symmetry may play a role when two degeneracy points formed by the same two states arrange themselves in symmetric positions with regard to a given symmetry line.[14] However, in general, these are, altogether, rare cases.

The RT intersections are known to be formed along the axes of collinear molecules and, consequently, the RT effect takes place when a potential energy surface (PES) of a given state splits upon bending into two PESs. The bending process happens when one atom (or more, in case of polyatomic systems) leaves the collinear axis and by doing that forms two states with different symmetries. Thus in case of a Π state and a triatomic molecule, we get for distances close enough to the collinear axis a pair of real electronic states: a symmetric state and an antisymmetric state (with respect to reflection in the molecular plane).

We studied so far two such molecules, namely, the earlier mentioned *triatomic system* (NH_2) and the tetra-atomic ($C_2H_2^+$) cation. In the case of NH_2, we revealed the resulting seam by shifting one of the atoms (either H or N) out of the (collinear) axis and calculated the topological phase by letting it surround the diatom axis formed by the two remaining atoms. This calculation yields, for not too large radii, the expected topological phase of $\sim 2\pi$.[1] Similar calculations were carried out for the tetra-cation, $C_2H_2^+$ (Ref. 2) (here the RT seam formed by the *collinear* tetra-atomic axes [see Fig. 1(a)] was revealed by removing an external hydrogen from the axis and allowing it to surround the collinear line formed by the remaining three CCH^+ atoms [see Fig. 1(b)]). As in the previous case, we found that the resulting topological phase is $\sim 2\pi$, which implies that the collinear tetra-atomic axis forms the expected RT intersections.[2–8] Next we shifted a hydrogen to a distance q_1 from the original axis and repeated the previous kind of calculations. We found, to our surprise, that for this situation, the topological phase is only $\sim \pi$ (and not 2π), which implies that the RT intersection changed its nature to become a *Jahn–Teller-type* of intersection. That *dramatic* change was verified for a series of situations as created by assuming different values for (q_1, q_2) [see Fig. 1(c)]. This unexpected result later caused Englman and Vertesi[15] to suggest, based on perturbation theory, that it is most likely that the *noncollinear* tetra-atomic configuration (for the $C_2H_2^+$ system) forms a second seam, which is

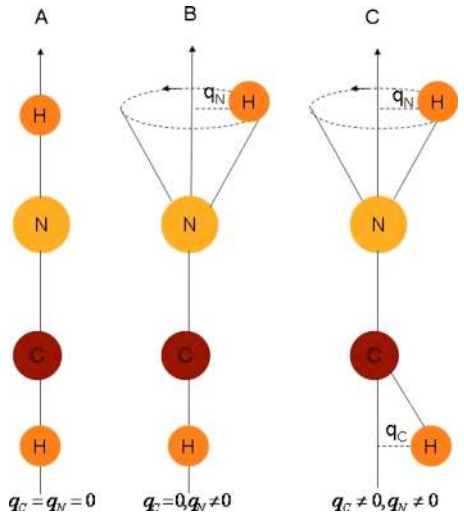

FIG. 1. The various configurations of a tetra-atomic system treated in the article: (a) the collinear tetra-atomic arrangement, (b) the *symmetric* case formed by a single atom surrounding the triatom axis, and (c) the nonsymmetric case formed by one shifted (clamped) atom and one atom surrounding the C–N axis.

located at another region in the configuration space. In other words, shifting an atom out from the collinear arrangements yields *two* JT seams: one along (or close to) the original tetra-atomic axis and another removed from the original axis and therefore missed by the surrounding contour. Shifting this atom back to its original position (thus forming again the tetra-atom collinear configuration) causes the two seams to *coalesce* and become one single seam. Recently Vibok and Halasz[16] extended the previously mentioned *ab initio* study[2] and revealed that, indeed, in case one atom is removed from the collinear tetra-atomic axis, the $C_2H_2^+$ system possesses two (and sometimes even three) nonoverlapping seams, as proposed by Englman and Vertesi.

The present article concentrates on another tetra-atomic RT-type molecule, namely, H_2CN. Initially we intended to study this molecule in order to reveal the extent of the similarity of its topological features with the previous tetra-atomic molecules. It will be shown that part of the features are, indeed, similar but then we found that H_2CN exemplifies interesting features of its own.

As mentioned earlier, our numerical study is based on *ab initio* NACTs as produced by MOLPRO.[17] The NACT, in general, is a *vectorial* entity that couples two given electronic adiabatic states so that if $\boldsymbol{\tau}_{jk}(\mathbf{s})$ is the term that couples states j and k, then it is written as[18]

$$\boldsymbol{\tau}_{jk}(\mathbf{s}) = \langle \zeta_j(\mathbf{s}_e|\mathbf{s}) | \nabla \zeta_k(\mathbf{s}_e|\mathbf{s}) \rangle, \tag{1}$$

where $\zeta_k(\mathbf{s}_e|\mathbf{s})$, $k=i,j$, are the electronic eigenfunctions, $\mathbf{s}$ and $\mathbf{s}_e$ stand for clusters of nuclear and electronic coordinates, respectively, and ∇ stands for the (nuclear) grad operator. In the present study, cylindrical coordinates are used; thus, $\mathbf{s}=(q,\varphi,z)$, where z is the (cylindrical) coordinate along the (collinear) axis of molecule and q and φ are the polar coordinates (q is the radius and φ is the angle) of an atom in a plane *perpendicular* to the molecular axis (see Fig. 1). As in previous studies, one atom is assumed to surround the molecular axis along a *circular* contour with its center

located on the axis. Of the various possible components of $\boldsymbol{\tau}_{jk}(\mathbf{s})$ that interests us is the angular component. Thus if φ is the angle associated with this (nuclear) rotation, then the corresponding angular component is written as $(1/\mathrm{q})\boldsymbol{\tau}_{\varphi jk}(\mathbf{s})$, where[9,10]

$$\tau_{\varphi jk}(\mathbf{s}) = \langle \zeta_j(\mathbf{s}_e|\mathbf{s}) | \frac{\partial}{\partial \varphi} \zeta_k(\mathbf{s}_e|\mathbf{s}) \rangle. \tag{2}$$

As mentioned above, we assume the four (collinear atoms) to be located along the z-axis with the origin being at some point along this axis [see Fig. 1(a)]. Throughout the numerical treatment, the carbon and the nitrogen form the (fixed) molecular axis and one of the hydrogens serves as the atom to surround the molecular axis. In the present study, we distinguish between two situations: (a) when the second hydrogen is clamped at a point on the CN axis (thus forming with the CN the triatomic axis [see Fig. 1(b)]) and (b) when the second hydrogen is clamped at a point shifted away from the CN axis [see Fig. 1(c)]. The first case is termed as the *symmetric* case and the second as the *nonsymmetric* case.

A. The ADT matrix A(s) and the topological matrix D(Γ)

In Ref. 2, the connection between the JT and RT frameworks is presented in detail, while justifying the application of the theory for the RT intersections originally developed for the JT intersections. This part will not be repeated here, but for the sake of completeness, we just list the main mathematical expressions to be used in this study.

Having the Born–Oppenheimer adiabatic (diagonal) potential matrix, $\mathbf{u}(\mathbf{s})$, the diabatic potential matrix $\mathbf{W}(\mathbf{s})$ is obtained following the ADT matrix $\mathbf{A}(\mathbf{s})$, [19(a)]

$$\mathbf{W}(\mathbf{s}) = \mathbf{A}^{\dagger}(\mathbf{s})\mathbf{u}(\mathbf{s})\mathbf{A}(\mathbf{s}). \tag{3}$$

The ADT matrix is an orthogonal (unitary) matrix that fulfills the following first-order differential (vector) equation:[19(a)]

$$\nabla \mathbf{A}(\mathbf{s}) + \boldsymbol{\tau}(\mathbf{s})\mathbf{A}(\mathbf{s}) = \mathbf{0}, \tag{4}$$

where $\boldsymbol{\tau}(\mathbf{s})$ is the nonadiabatic coupling *matrix* (NACM) with the elements as defined in Eq. (1). The solution of this equation can be written as an exponentiated line integral[20(a),20(b)]

$$\mathbf{A}(\mathbf{s}|\mathbf{s}_0,\Gamma) = \wp \exp\left(- \int_{\mathbf{s_0}}^{\mathbf{s}} d\mathbf{s} \cdot \boldsymbol{\tau}(\mathbf{s}|\Gamma) \right) \mathbf{A}(\mathbf{s}_0), \tag{5}$$

where $\wp$ is the *ordering* operator, s_0 is the initial point of integration, Γ is the contour along which Eq. (4) is required to be solved, the dot stands for a scalar product, and $\mathrm{A}(\mathbf{s}_0)$ is the initial value of $\mathrm{A}(\mathbf{s})$ on Γ. In what follows, $\mathrm{A}(\mathbf{s}_0)$ is assumed to be the *unit* matrix.

Another matrix of interest is the *topological* matrix $\mathbf{D}(\Gamma)$, which is identical to the $\mathbf{A}$ matrix but is calculated along *closed* contours[21(a)–21(c)]

$$\mathbf{D}(\Gamma) = \mathbf{A}(\mathbf{s}_0|\mathbf{s}_0,\Gamma) = \wp \exp\left(- \oint_{\Gamma} d\mathbf{s} \cdot \boldsymbol{\tau}(\mathbf{s}|\Gamma) \right). \tag{6}$$

The $\mathbf{D}$-matrix does not depend on any specific point along Γ but on the contour as a whole. It can be shown that in order for the diabatic potential matrix $\mathbf{W}(\mathbf{s})$ [see Eq. (3)] to be *single-valued* in a region of interest, the $\mathbf{D}$-matrix has to be *diagonal* for any chosen closed contour Γ in that region.[21(b),21(c)] Since $\mathbf{D}(\Gamma)$ [just like $\mathbf{A}(\mathbf{s})$] is unitary, its elements are expected to be

$$\mathbf{D}_{jk}(\Gamma) = \delta_{jk} \exp(i\theta_j(\Gamma)), \quad j = \{1,N\}, \tag{7}$$

where $\theta_j(\Gamma)$, $j=\{1,N\}$, are real phases. In the case of real *eigenfunctions*, the phases become integer multiples of π so that the $\mathbf{D}$-matrix elements are

$$\mathbf{D}_{jk}(\Gamma) = \pm \delta_{jk}, \quad j = \{1,N\}. \tag{8}$$

Since the single-valuedness is solely determined by the NACM, it is noticed that in order for a group of N states to yield single-valued diabatic potentials, all that is necessary is to calculate the corresponding $\mathbf{D}$-matrix and see to what extent it is diagonal.

In the case of circular contours, Eqs. (5) and (6) are simplified to become[19(b)]

$$\mathbf{A}(\varphi|\mathrm{q},\Gamma) = \wp \exp\left(- \int_0^{\varphi} d\varphi \boldsymbol{\tau}_{\varphi}(\varphi|\mathrm{q},\Gamma) \right) \tag{9}$$

and

$$\mathbf{D}(\mathrm{q},\Gamma) = \wp \exp\left(- \int_0^{2\pi} d\varphi \boldsymbol{\tau}_{\varphi}(\varphi|\mathrm{q},\Gamma) \right), \tag{10}$$

respectively [where $\boldsymbol{\tau}_{\varphi}$ is a matrix that contains elements defined in Eq. (2)].

In the case of the two states, Eqs. (9) and (10) are simplified significantly because any 2×2 orthogonal matrix can be written as

$$\mathbf{A}^{(2)}(\varphi,\mathrm{q}) = \begin{pmatrix} \cos(\gamma_{12}(\varphi,\mathrm{q})) & \sin(\gamma_{12}(\varphi,\mathrm{q})) \\ -\sin(\gamma_{12}(\varphi,\mathrm{q})) & \cos(\gamma_{12}(\varphi,\mathrm{q})) \end{pmatrix}, \tag{11}$$

where $\gamma_{12}(\varphi,\mathrm{q})$ is the ADT angle (known also as the mixing angle) expressed in terms of a line integral[19]

$$\gamma_{12}(\varphi,\mathrm{q}) = \int_0^{\varphi} \boldsymbol{\tau}_{\varphi 12}(\varphi',\mathrm{q})\mathrm{d}\varphi'. \tag{12}$$

A similar expression is given for $\alpha_{12}(\mathrm{q})$, which is the topological phase (*the-end-of-the-contour*-ADT), namely,[21]

$$\alpha_{12}(\mathrm{q}) = \int_0^{2\pi} \boldsymbol{\tau}_{\varphi 12}(\varphi',\mathrm{q})\mathrm{d}\varphi'. \tag{13}$$

The corresponding $\mathbf{D}$-matrix is similar to the $\mathbf{A}$-matrix given in Eq. (11), with $\gamma_{12}(\varphi,\mathrm{q})$ is replaced by $\alpha_{12}(\mathrm{q})$, namely,

$$\mathbf{D}^{(2)}(\mathrm{q}) = \begin{pmatrix} \cos(\alpha_{12}(\mathrm{q})) & \sin(\alpha_{12}(\mathrm{q})) \\ -\sin(\alpha_{12}(\mathrm{q})) & \cos(\alpha_{12}(\mathrm{q})) \end{pmatrix}. \tag{14}$$

It is well noticed that the condition for the $\mathbf{D}$-matrix to be *diagonal* is that

$$\alpha_{12}(\mathrm{q}) = 2\pi n, \tag{15}$$

where n is an integer or half integer.[21(a),21(b)] Next, since we consider only the *angular* component of $\boldsymbol{\tau}$, we drop the subscript φ but remember that $\boldsymbol{\tau}$ and $\boldsymbol{\tau}_{jk}$ stand for $\boldsymbol{\tau}_{\varphi}$ and $\boldsymbol{\tau}_{\varphi jk}$, respectively.

B. Treatment of symmetrical NACTs

One of the features that characterize the treatment of the RT intersection is that frequently their NACTs can be chosen to be independent of the polar angle φ. This happens when the *centers* of the circular contours Γ are located at the molecular axis and for situations as presented in Fig. 1(b) [in contrast to situations that are presented in Fig. 1(c)]. In such a case, we find that due to this symmetry, the integration of Eqs. (9), (10), (12), and (13) can be carried out trivially. In what follows, we briefly refer analytically to two specific cases.

1. The two-state Hilbert subspace

In this case the $\boldsymbol{\tau}$-matrix is of the form

$$\boldsymbol{\tau}(\mathrm{q}) = \begin{pmatrix} 0 & 1 \\ -1 & 0 \end{pmatrix} \tau_{12}(\mathrm{q}), \tag{16}$$

and since $\boldsymbol{\tau}_{12}$ does not depend on the angle φ, the corresponding **D**-matrix becomes [see Eq. (14)]

$$\mathbf{D}^{(2)}(\mathrm{q}) = \begin{pmatrix} \cos(2\pi\tau_{12}) & \sin(2\pi\tau_{12}) \\ -\sin(2\pi\tau_{12}) & \cos(2\pi\tau_{12}) \end{pmatrix}. \tag{17}$$

In order for the **D**-matrix to be diagonal, $\boldsymbol{\tau}_{12}$ has to fulfill the condition

$$\tau_{12}(\mathrm{q}) = \begin{cases} n & \text{(a)} \\ (2n+1)/2 & \text{(b)}, \end{cases} \tag{18}$$

where n is an integer. In other words, the two states under consideration form a Hilbert *subspace* in a region defined by q if and only if for each q-value in that region n is an integer. It is important to mention that case (a) applies to a parabolic (RT) intersection and case (b) with $n=0$ applies to a conical (JT) intersection (not considered in the present article).

2. The tristate Hilbert subspace

Here, like in the previous case, the $\boldsymbol{\tau}$-matrix elements do not depend on φ so that the **D**-matrix takes the form [see Eq. (10)]

$$\mathbf{D}(\mathrm{q}) = \exp(-2\pi\boldsymbol{\tau}(\mathrm{q})). \tag{19}$$

To treat the three-state case, we assume the 3×3 $\boldsymbol{\tau}$-matrix to be of the simplified) form

$$\boldsymbol{\tau}(\mathrm{q}) = \begin{pmatrix} 0 & \tau_{12}(\mathrm{q}) & 0 \\ -\tau_{12}(\mathrm{q}) & 0 & \tau_{23}(\mathrm{q}) \\ 0 & -\tau_{23}(\mathrm{q}) & 0 \end{pmatrix}, \tag{20}$$

so that $\tau_{13}(\mathrm{q})$ is assumed to be negligibly small. It is important to note that we make this assumption just to derive simpler expressions for the analytic presentation (in the *numerical* part all three elements are considered).

Next, substituting Eq. (20) into Eq. (19) yields the following **D**-matrix:[2,21(a)–21(c)]

$$\mathbf{D}^{(3)}(\mathrm{q}) = \omega^{-2} \begin{pmatrix} \tau_{23}^2 + \tau_{12}^2\mathrm{C} & \tau_{12}\omega\mathrm{S} & \tau_{12}\tau_{23}(1-\mathrm{C}) \\ \tau_{12}\omega\mathrm{S} & \omega^2\mathrm{C} & -\tau_{23}\omega\mathrm{S} \\ \tau_{12}\tau_{23}(1-\mathrm{C}) & \tau_{23}\omega\mathrm{S} & \tau_{12}^2 + \tau_{23}^2\mathrm{C} \end{pmatrix}, \tag{21}$$

where

$$\mathrm{C} = \cos(2\pi\omega), \quad \mathrm{S} = \sin(2\pi\omega), \quad \omega = \sqrt{\tau_{12}^2 + \tau_{23}^2}, \tag{22}$$

and we recall that $\tau_{jk} \equiv \tau_{jk}(\mathrm{q})$. It is well noticed that the $\mathbf{D}^{(3)}$-matrix in Eq. (21) becomes diagonal if and only if $\omega=n$, where n is an integer.

Since our main concern is the diagonal elements of the $\mathbf{D}^{(3)}$-matrix, we calculate them employing the following expressions:

$$(\mathrm{D}_{11}^{(3)}, \mathrm{D}_{22}^{(3)}, \mathrm{D}_{33}^{(3)}) = \left(\frac{\tau_{12}^2\mathrm{C} + \tau_{23}^2}{\tau_{12}^2 + \tau_{23}^2}, \ \mathrm{C}, \ \frac{\tau_{12}^2 + \tau_{23}^2\mathrm{C}}{\tau_{12}^2 + \tau_{23}^2} \right). \tag{23}$$

It is noticed that for those cases for which ω is an integer all three diagonal elements are equal to 1.

3. Short summary

In Sec. I B, we analyzed the two-state case and the three-state case. For the two-state case, we found that the single-valued diabatization in a given region is valid as long as $\tau_{12}(\mathrm{q})=n$, where n is an integer, which is a result known for quite some time.[9,10] As for the three-state diabatization, here we encountered a new condition. We found that a three-state single-valued diabatization in a given region is valid if and only if $\omega(\mathrm{q})$, as defined in Eq. (22), is an *integer*.

C. Treatment of nonsymmetrical NACTs

Nonsymmetrical NACTs are formed when one of the (four) atoms is shifted away from the collinear axis [see Fig. 1(c)]. As already mentioned earlier, the two central atoms, C and N form the *fixed* axis and the two external atoms (in this case, the two hydrogens) are the ones to be shifted away from this axis. One of the hydrogens (on the carbon side and labeled as $\mathrm{H_C}$) is shifted to a fixed distance $\mathrm{q_C}$ from the CN axis and clamped at a fixed angle φ to be defined as $\varphi=0$. The other hydrogen (on the nitrogen side and labeled as $\mathrm{H_N}$) is the atom assumed to surround the CN axis with a fixed radius $\mathrm{q_N}$.

The nonsymmetrical case is characterized by the fact that the NACTs *do depend* on the angle φ and therefore the calculations involve integrations over that angle. As long as the two-state NACTs suffice for obtaining the information concerning the lower RT intersections in a given region, the calculations are simple and straightforward. However, the present molecule (in contrast to the previous $\mathrm{C_2H_2^+}$ cation) was found to be more complicated because the two-state results were not satisfying and we soon had to treat tristate NACTs. This situation requires the application of 3×3 $\mathbf{A}(\varphi,\mathrm{q})$ and $\mathbf{D}(\Gamma)$ matrices (as is done routinely in JT systems) but, as will be shown, even this information is not always conclusive regarding lower-state-Renner–Teller intersections. Consequently, we had to apply more sophisticated

means in order to be more conclusive on the issues at stake. This is what is done next.

Just like in the two-state case, we take advantage of the fact that the **A**-matrix is an orthogonal matrix and, therefore, its nine elements can be presented in terms of three angles, reminiscent of the Euler angles.[22,23] This idea was already discussed, applied, and analyzed in a series of articles[22] and again is only briefly discussed here.

As in the case of the ordinary Euler (three-dimensional) matrix, the orthogonal **A**-matrix is presented as a product of *three rotation* matrices $\mathbf{Q}_{ij}(\gamma_{ij})$ $(i<j=2,3)$, where the product $\mathbf{A}=\mathbf{Q}_{kl}\mathbf{Q}_{mn}\mathbf{Q}_{pq}$ can be written in any order. Substituting this product into Eq. (4) yields three coupled first-order differential equations for the three corresponding quasi-Euler angles, γ_{ij}. The final set of equations, as well as their solution, depends on the order of the **Q**-matrices[22(b)] (there exist six different products).

In an analysis carried out several years ago,[22(a),22(c),22(e)] we attributed physical meanings only to those ADT angles γ_{ij}, *privileged* with equations where their corresponding NACT, τ_{ij}, are a free *isolated* term. In Ref. 22(c), we showed that in order to ensure a privileged angle γ_{ij}, we have to consider **A**-matrices (with N dimension) of the kind

$$\mathbf{A}^{(N)}(\gamma_{12},\gamma_{13},\ldots)=\mathbf{Q}^{(N)}(\gamma_{ij})\tilde{\mathbf{A}}^{(N)}(\gamma_{13},\gamma_{23},\ldots),$$

where $\tilde{\mathbf{A}}^{(N)}(\gamma_{13},\gamma_{23},\ldots)$ is formed by products of all the relevant Euler-type matrices except for the one defined in terms of γ_{ij}. In the case of $N=3$, there are two such matrices for each angle. In what follows, we consider the two matrices for γ_{12}.

(a) For the product $\mathbf{A}=\mathbf{Q}_{12}\mathbf{Q}_{13}\mathbf{Q}_{23}$, we get the following set of equations for which γ_{12} [Ref. 22(a)] is the privileged angle:

$$\begin{aligned}\nabla\gamma_{12}&=-\tau_{12}-\tan\gamma_{13}(\tau_{23}\cos\gamma_{12}+\tau_{13}\sin\gamma_{12}),\\ \nabla\gamma_{23}&=\tau_{23}\sin\gamma_{12}-\tau_{13}\cos\gamma_{12},\\ \nabla\gamma_{13}&=-(\cos\gamma_{13})^{-1}(\tau_{23}\cos\gamma_{12}+\tau_{13}\sin\gamma_{12}).\end{aligned}\tag{24}$$

(b) For the product $\mathbf{A}=\mathbf{Q}_{12}\mathbf{Q}_{23}\mathbf{Q}_{13}$, we get another set of equations[22(b),22(c)] for which γ_{12} [Ref. 22(a)] is the privileged angle

$$\begin{aligned}\nabla\gamma_{12}&=-\tau_{12}-\tan\gamma_{23}(-\tau_{13}\cos\gamma_{12}+\tau_{23}\sin\gamma_{12}),\\ \nabla\gamma_{23}&=-(\tau_{23}\cos\gamma_{12}+\tau_{13}\sin\gamma_{12}),\\ \nabla\gamma_{13}&=(\cos\gamma_{23})^{-1}(-\tau_{13}\cos\gamma_{12}+\tau_{23}\sin\gamma_{12}).\end{aligned}\tag{25}$$

Next, we make the connection between the privileged angle γ_{12} and the corresponding Berry phase. Following the seminal article of Berry,[24(a)] one of the present authors and Englman suggested to identify the *two-state* Berry phase with the *end-of-the-contour angle* as obtained from a *two-state* calculation[24(b)] [see Eqs. (12) and (13)]. This definition was found to be internally consistent in numerous studies related to Hilbert subspaces with two quasi-isolated states (in a given region).[9,10,13,25]

This definition had to be modified in the case of a Hilbert subspace with three [or more) strongly coupled states (we recall that the Berry phase applies for any number of states[24(a)]]. A natural possibility is to consider the ADT (mixing) angle γ_{12} as introduced either by Eq. (24) or Eq. (25) and assigning the required Berry phase as the *end-of-the-contour* value, α_{12}. Assuming the closed contour is Γ, we define $\alpha_{12}=\gamma_{12}(\Gamma)$. In the same way, if we consider a set of equations with some other privileged mixing angle γ_{mn}, then the corresponding Berry phase α_{mn} is given by $\gamma_{mn}(\Gamma)$.

II. NUMERICAL RESULTS

In this article, a detailed study of H_2CN is presented. Four types of results are considered: (a) energy curves, (b) angular NACTs, (c) diagonal **A**-(ADT) and **D**-matrix elements, and (d) the (1,2) mixing angles γ_{12} and the corresponding topological phases α_{12}. The calculations are done for two types of configurations as described in Fig. 1(b) (the symmetric case) and Fig. 1(c) (the nonsymmetric case) and as elaborated earlier in Secs. I B and I C, respectively. Therefore the present chapter is constructed in a similar way. All calculated magnitudes are presented as a function of cylindrical coordinates where the z-coordinates for the four atoms are fixed.

The calculations of adiabatic potential energy curves and the angular NACTs were done employing the MOLPRO program[17] at the state average complete active space self-consistent field (CASSCF) level, using the 6-311G** basis set for all atoms. The active space was constructed by distributing eleven valence electrons in ten orbitals. In the state average-CASSCF calculation were taken six electronic states with equal weights. All calculations were done for the following collinear configuration: the C–N distance: $R_{CN}=1.22$ Å, the H–C distance: $R_{HC}=1.11$ Å, and the H–N distance: $R_{HN}=1.03$ Å.

A. Treatment of the symmetrical case

As already mentioned earlier, the symmetrical case is formed when one hydrogen is allowed to surround the triatomic axis along a closed circular contour with its center on the axis [see Fig. 1(b)]. We distinguish between two situations, namely, when H_C serves as the atom to surround the triatom axis and when H_N serves as the surrounding atom.

So far, only systems that include either two states or three states were mentioned. In this section, we consider also systems with four states with the aim of showing the convergence rate of certain magnitudes.

Figures 2(a) and 2(b) present the energy curves for these two situations. The two lower curves stand for the two states, $1\,^2A'$ and $1\,^2A''$, which evolve from the collinear $X\,^2\Pi$-state, and the third and the fourth curves evolved from the collinear $1\,^2\Sigma^+$ and $2\,^2\Sigma^+$ states and are labeled as $2\,^2A'$ and $3\,^2A'$. We use this notation to emphasize the fact that A'-states interact with A''-states and therefore $1\,^2A''$ is expected to interact with all three A'-states, namely, $1\,^2A'$, $2\,^2A'$, and $3\,^2A'$.

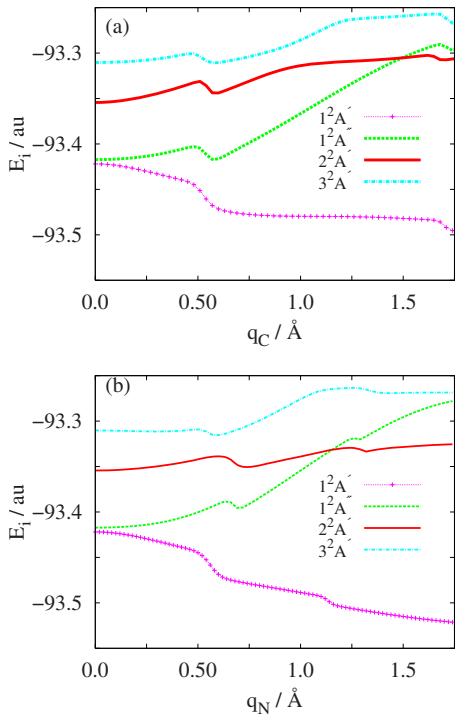

FIG. 2. Energy curves as a function of q (symmetric case) related to four electronic states: the 1 ^{2}A′ state, the 1 ^{2}A″ state (both evolving from the two degenerate X $^2\Pi$-state), and the third and the fourth states that evolve from the (collinear) 1 $^2\Sigma^+$ and 2 $^2\Sigma^+$ states to become the 2 ^{2}A′ and 3 ^{2}A′. These four states are the lower ones for the collinear arrangement and at regions close to it. (a) The $H_C\cdots CNH_N$ system (H_C is the rotating atom). (b) The $H_CCN\cdots H_N$ system (H_N the rotating atom).

Figures 3(a) and 3(b) present the three relevant NACTs: $\tau_{12}(q)$, $\tau_{23}(q)$, and $\tau_{24}(q)$ for the above-mentioned situations. Figure 3(a) present the results for H_C as the surrounding atom and in Fig. 3(b) for the H_N surrounding atom.

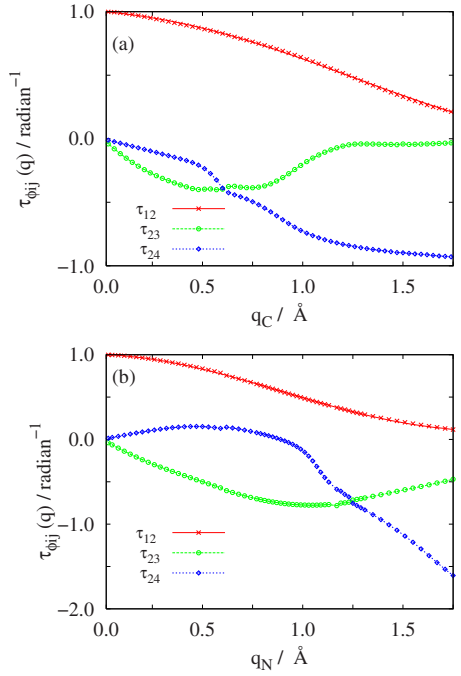

FIG. 3. Renner–Teller angular nonadiabatic coupling terms (symmetric case) as a function of q. (a) The $H_C\cdots CNH_N$ system (H_C the rotating atom). (a) The $H_CCN\cdots H_N$ system (H_N the rotating atom).

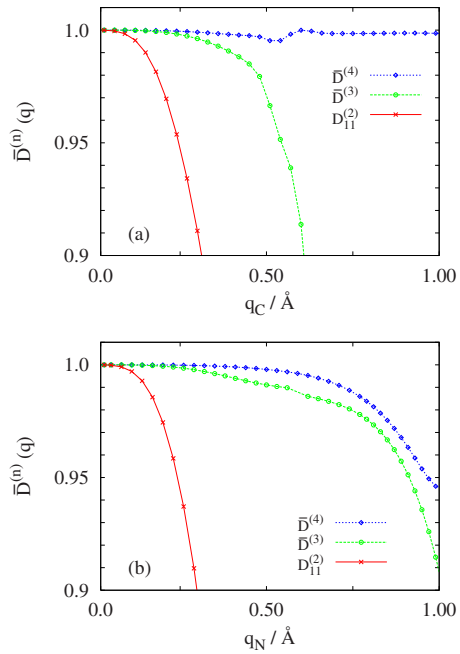

FIG. 4. Two-state, tristate, and tetrastate **D**-matrix elements (symmetric case). Three curves are shown in each panel: one presents the (1,1) elements of $\mathbf{D}^{(2)}$ and the other two present the elements $\bar{D}^{(n)}(q)$; $n=3,4$ [see Eq. (26)] related to the matrices $\mathbf{D}^{(3)}$ and $\mathbf{D}^{(4)}$, respectively. (a) The $H_C\cdots CNH_N$ system (H_C the rotating atom). (b) The $H_CCN\cdots H_N$ system (H_N the rotating atom).

Figures 4(a) and 4(b) present the geometric means of the diagonal **D**-matrix elements again for the two abovementioned situations. Results are shown for the two-state, tristate, and tetrastate calculations.

We remind the reader that in order to have a single-valued diabatization, the **D**-matrix has to be diagonal and its elements have to be equal to ± 1. However, since the study concentrates on the RT intersections, it was shown that all diagonal elements have to be equal to +1 (Refs. 1 and 2) (see Sec. I B). In other words, the **D**-matrix for the RT system is expected to be as close as possible to the unit matrix.

We start the analysis for the two-state case. Following Eq. (17), it is noticed that $D^{(2)}_{11}(q)\equiv D^{(2)}_{22}(q)$ and therefore it is enough to show only one matrix element (the upper index designates the dimension of the **D**-matrix). It is clearly seen [in both Figs. 4(a) and 4(b)] that the values of $D^{(2)}_{11}(q)$ are close to 1 only along a short range ($q\leq 0.15$ Å) and from thereon the deviations from +1 increase as q gets larger. Thus, for instance, at $q\sim 0.4$ Å, we encounter, for $D^{(2)}_{11}(q)$ the value ~ 0.80. The reason is due to the deterioration of $\tau_{12}(q)$, which is expected to be ~ 1, but, in fact, decreases uniformly as q increases. For instance, at $q=0.4$ Å, it drops to ~ 0.9 [see Fig. 3(a) as well as Fig. 3(b)] and causes $D^{(2)}_{11}(q=0.4$ Å) to become 0.8 (in both cases)

More encouraging results are obtained in case we include three or four states in the calculations. Since the **D**-matrices are expected to be unit matrices, we show, for these multistate matrices, the corresponding geometrical mean of their diagonal elements. Thus in the case of n (=3,4) states, the corresponding average value $\bar{D}^{(n)}(q)$ is defined as[2(a)]

$$\bar{D}^{(n)}(q) = \sqrt[n]{\prod_{j=1}^{n} D_{jj}^{(n)}(q)}, \quad n = 3,4. \tag{26}$$

The expected value (in case of convergence) is 1. From Eq. (23), it can be seen that in order for $\bar{D}^{(n=3)}(q)=1$, the value of ω, defined as $\omega=\sqrt{\tau_{12}^2+\tau_{23}^2}$ [see Eq. (22)], has to be an integer, i.e., $\omega \sim n$. Similar expressions can be derived for higher dimensions.

Returning now to Figs. 4(a) and 4(b), the second curve in each figure represents the results due to a tristate calculation. It is noticed that adding the third state indeed improved the situation by guaranteeing the unit feature of the **D**-matrices for a larger interval: in case the rotating atom is H_C, the interval extends from ~0.15 Å to ~0.5 Å, and in case it is H_N, it extends from ~0.15 to ~0.6 Å. Adding another state (so that $n=4$) improves the quality of the **D**-matrix elements up to q-values beyond this range (in case of H_C the interval reaches q-values beyond the figure).

B. Treatment of the nonsymmetrical case

The nonsymmetrical case is described in Fig. 1(c) and the results are presented in Figs. 5–10. As mentioned earlier, we treat here the situations where the axis is formed by carbon and nitrogen only and the two hydrogens are shifted away from this axis. We distinguish between two cases. (i) H_C is clamped to its position at $\varphi=0$ and H_N is allowed to surround the axis along a circular contour with its center on the axis. (ii) H_N is clamped to its position at $\varphi=0$ and H_C is allowed to surround the axis, again, with its center on the axis. In this way, the magnitudes of interest—see below—depend on the two distances q_C and q_N, and the angle φ, which is the angle between two planes, NCH_C and H_NNC. In addition, these magnitudes (as already mentioned earlier) depend also on three distances along the NC axis, which are held fixed throughout this study.

In general, we distinguish between two types of results. (a) Local results that depend on the three abovementioned coordinates (q_C, q_N, and φ). This type includes the potential energies, the NACTs, the diagonal ADT matrix elements, and the ADT (or the mixing) angles γ_{12} [see Eqs. (12), (24), and (25)]. (b) *Contour-dependent* results (i.e., the topological results) such as the **D**-matrix elements and the corresponding phases α_{12} that depend on (q_C, q_N) only.

In this section, we concentrate on the three lower states of the bent HCNH molecule, namely, the states $1\,^2A'$ and $1\,^2A''$ (which in the linear point group $C_{\infty v}$ configuration correspond to the two degenerate $1\,^2\Pi$ states), and one additional A′ state, namely, the $2\,^2A'$ state that evolves from the linear $1\,^2\Sigma^+$ state.

The results in general *do not* depend on which of the atoms is the rotating atom and which is the clamped one. This is obvious for the local results but it applies also to the topological results. The study to be described next is divided into two parts: part A where $q_C<q_N$ and part B where $q_C>q_N$. In part A, we consider four different combinations of (q_C,q_N), namely, (q_C,q_N) $=\{(0.01,0.2);(0,02,0.6);(0.2,0.6);(0.4,0.6)\}$ Å, and in part B, we consider two such combinations, namely, $(q_C,q_N)=\{(0.1,0.01);(0.6,0.2)\}$.

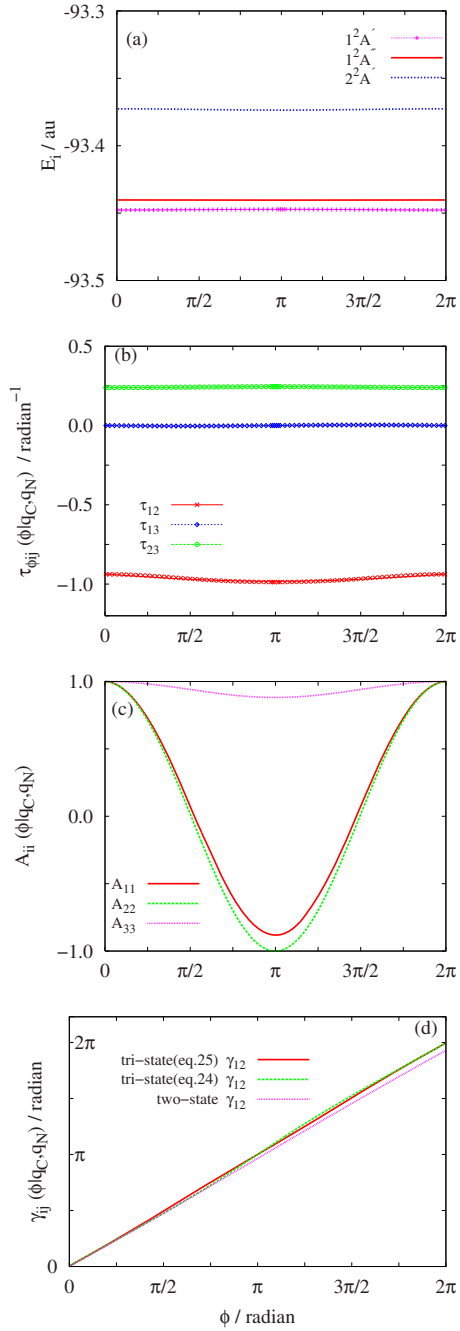

FIG. 5. Summary of results (nonsymmetric case) obtained for the rotating hydrogen H_N and the clamped (shifted) hydrogen H_C. Results are shown in four panels. Panel (a) presents energy curves related to the three mentioned states in the panel. Panel (b) presents angular NACTs, $\tau_{ij}(\varphi|q_C,q_N)$ as mentioned in the panel. Panel (c) presents the diagonal matrix elements $\mathbf{A}_{jj}(\varphi|q_C,q_N)$ $\{j=1,3\}$ of the ADT matrix. Panel (d) presents the ADT angle $\gamma_{12}(\varphi|q_C,q_N)$ as obtained in three different calculations (see text). The results are presented as a function of φ calculated for $q_N=0.2$ Å and $q_C=0.01$ Å.

Figures 5–8 present the results related to part A and Figs. 9 and 10 present the results for part B. In panel (a) of each figure, the (three) energy curves $E_{1A'}(\varphi|q_C,q_N)$, $E_{1A''}(\varphi|q_C,q_N)$, and $E_{2A'}(\varphi|q_C,q_N)$ are presented. In panel (b), the three corresponding NACTs, $\tau_{12}(\varphi|q_C,q_N)$, $\tau_{23}(\varphi|q_C,q_N)$, and $\tau_{13}(\varphi|q_C,q_N)$ are presented. In panel (c),

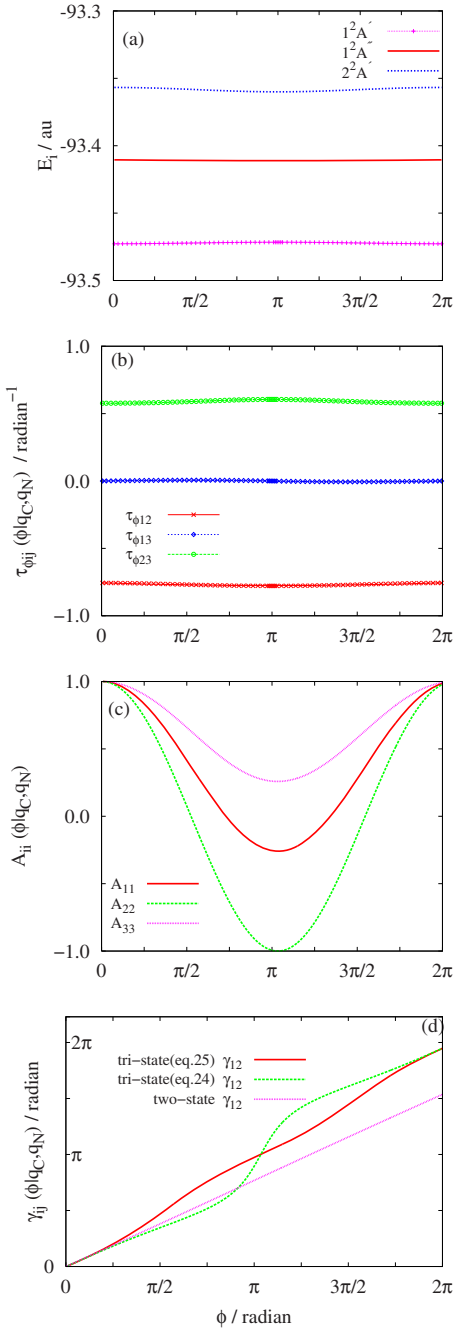

FIG. 6. The same as Fig. 5 but for q_N=0.6 Å and q_C=0.02 Å.

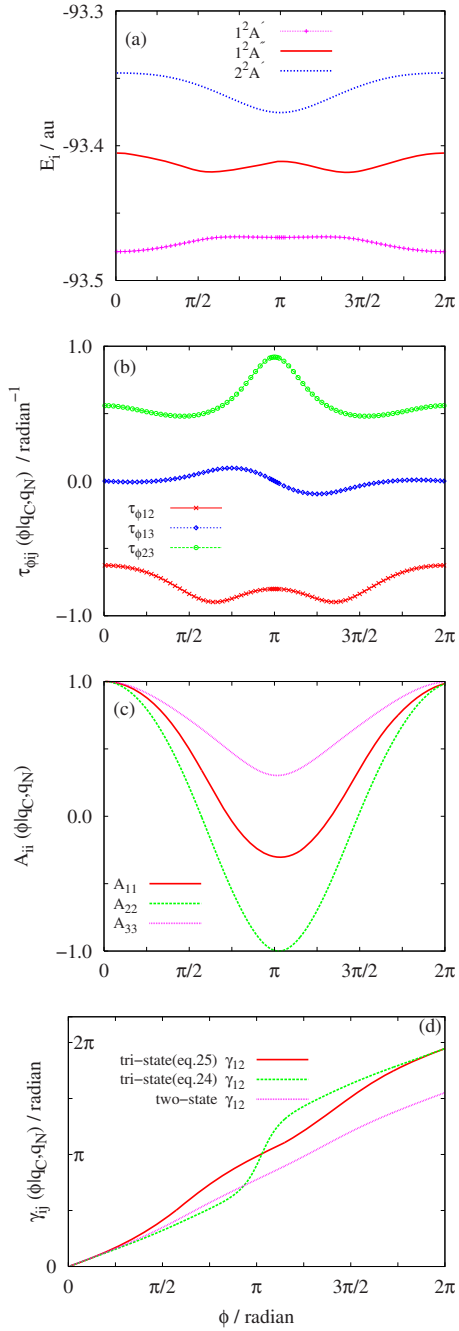

FIG. 7. The same as Fig. 5 but for q_N=0.6 Å and q_C=0.2 Å.

the diagonal elements of the corresponding **A**-matrices, $A_{11}(\varphi|q_C,q_N)$, $A_{22}(\varphi|q_C,q_N)$, and $A_{33}(\varphi|q_C,q_N)$ are presented and in panel (d), the two-state ADT angles $\gamma_{12}(\varphi|q_C,q_N)$ calculated by solving Eq. (12) and the two tristate ADT angles $\gamma_{12}(\varphi|q_C,q_N)$ calculated once by solving Eq. (24) and once by solving Eq. (25) are presented.

In general, the results show weak dependence on φ (in particular, when one of the two distances is small). The dependence on φ becomes stronger as the smaller distance of the two increases.

The values α_{12} of the topological (Berry) phases as calculated for the various cases are presented in Table I. The expected value is 2π and it is noticed that as long as the *two* distances q_C and q_N are small enough, the deviations from 2π are slight. However, when at least one of the distances increases significantly, the deviations become apparent, in particular, for the two-state treatment (however, all values are in the proximity of 2π).

We present in six figures almost *similar* results and the reason for that is to convince the reader that the *novel* Berry phases as obtained in these six significantly different situations are not accidental but demonstrate *internal* consistency. We showed here as well as in previous articles[1,2] that RT intersections yield **D**-matrices that are unit matrices. Thus the results of having unit **D**-matrices and Berry phases being $\sim 2\pi$ are consistent.

III. CONCLUSIONS

The study presented in this article can be considered as a continuation of a previous study carried out for the $C_2H_2^+$

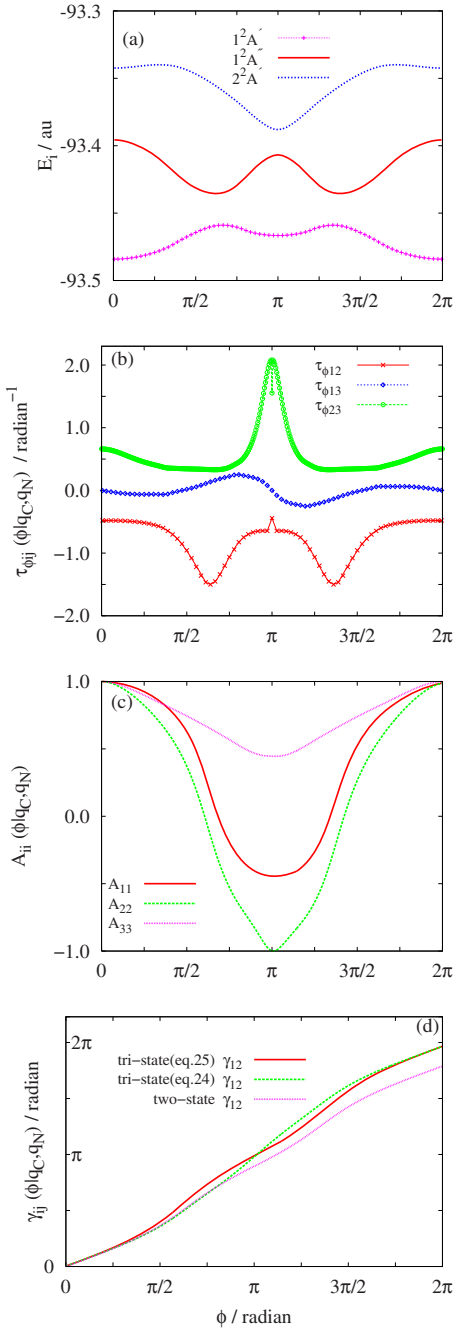

FIG. 8. The same as Fig. 5 but for q_N=0.6 Å and q_C=0.4 Å.

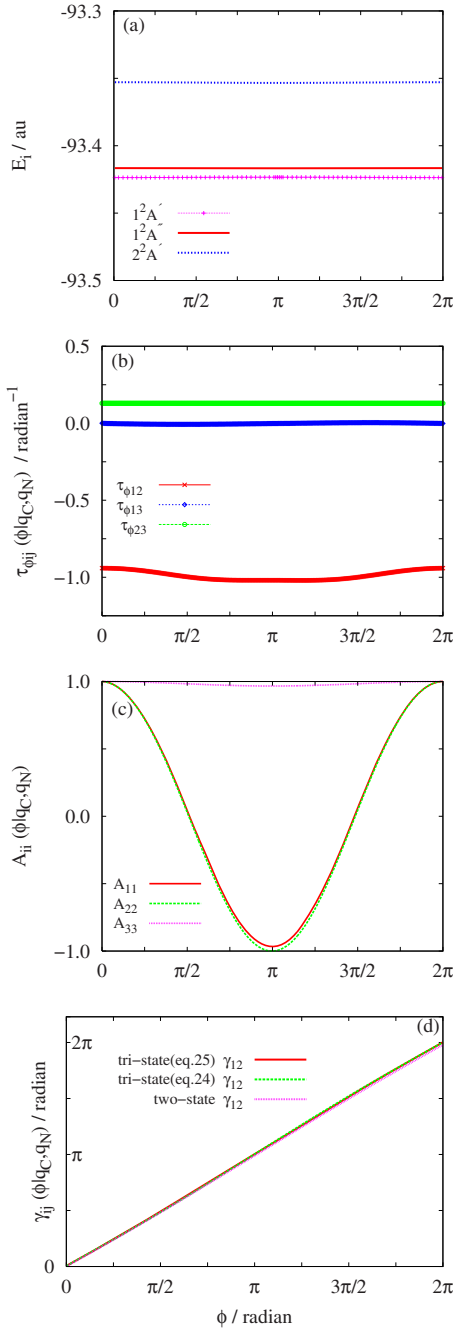

FIG. 9. Summary of results (nonsymmetric case) obtained for the rotating hydrogen H_C and the clamped (shifted) hydrogen H_N. The rest is the same as Fig. 5 but for q_N=0.01 Å and q_C=0.1 Å.

cation.[2] To some extent, the findings are similar but there are also significant differences. We start by briefly summarizing the main features that are common to the two studies and then refer to the differences between them.

The fact that a tetra-atomic system contains more atoms than the triatomic system provides additional possibilities, which make their study more interesting. In the case of a triatomic system, topological RT effects are revealed when one atom surrounds the axis formed by the two other atoms.[1] In the case of tetra-atomic systems, topological effects are revealed when one atom surrounds the *triatom* axis, namely, the so called symmetrical case [Fig. 1(b)] or when it surrounds an axis formed by two atoms and the third atom is shifted away from that axis, namely, the nonsymmetrical case [Fig. 1(c)].

The similarity between the two tetra-atomic studies is that for the symmetrical case, they both supply the expected results, namely, they reveal the existence of RT intersections along the collinear arrangement (which is characterized by the fact that the **D**-matrices are unit matrices). We may go one step further and say that the two studies yield similar results even for the nonsymmetrical cases in the sense that they both reveal the existence of *seams* of degeneracy points along the remaining triatomic axis. In other words shifting one atom away from the collinear axis is not enough to *abolish* topological effects produced by the *original* tetra-atomic axis (and in this sense the two systems are similar). However, as already elaborated in the Introduction, our previous

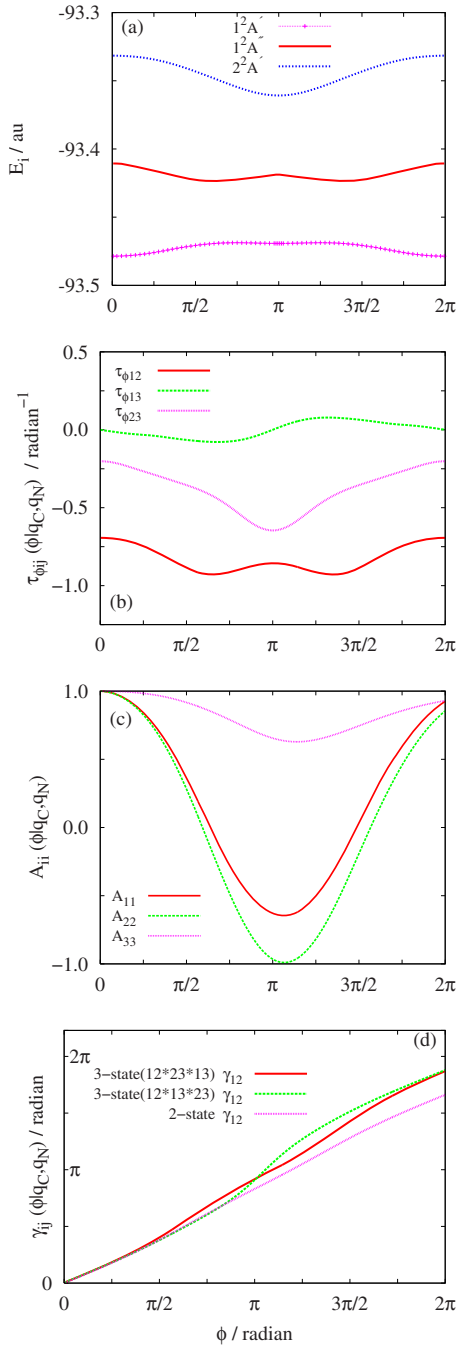

FIG. 10. The same as Fig. 9 but for q_N=0.2 Å and q_C=0.6 Å.

study (on the $C_2H_2^+$ ion) indicated that for the nonsymmetrical case the remaining collinear triatom axis becomes a line (seam) of JT conical intersection, thus yielding a nonunit **D**-marix (namely, $D_{11}=D_{22}=-1$ and $D_{33}=1$). Here, for the H_2CN molecule, we find that shifting one atom away from collinearity leaves the RT intersection unchanged. In other words, the collinear tetra-atomic and the collinear triatomic axes both form unit **D**-matrices.

We did not pursue this study to find out why the two tetra-atomic systems behave so differently for the nonsymmetrical case. It could very well be that this behavior is associated with the strength of the hydrogen bonds of the two molecules. Since the hydrogen bonds in the case of H_2CN are much stronger, it is expected that this molecule is more robust and therefore is likely to maintain its topological features in more extreme situations.

TABLE I. Topological (Berry) phases.

Shift (Å)	q_C	q_N	Two-state Equation (12)	Three-state Equation (24)	Three-state Equation (25)
A[a]	0.01	0.2	6.06	6.27	6.27
	0.02	0.6	4.83	6.12	6.12
	0.2	0.6	4.87	6.11	6.11
	0.4	0.6	5.00	6.13	6.13
B[b]	0.1	0.01	6.22	6.28	6.28
	0.6	0.2	5.22	5.90	5.87

[a]A applies to $q_N > q_C$.
[b]B applies to $q_N < q_C$.

Finally we elaborate briefly on the new definition of the (topological) Berry phases in case of three interacting states. So far Berry phases, within the time-*independent* formulation, are well defined for two isolated interacting states only.[9,10] In the present study we established for the first time that the mixing angles $\gamma_{12}(\varphi|q_C,q_N)$, as obtained by solving Eqs. (24) and (25), may yield meaningful physical phases α_{12} that could be identified as the Berry phases for situations where three states are strongly interacting. The fact that the concept of topological phase still pertains in such situations it becomes important to determine the fate of *degeneracy* lines (seams) due to the additional interactions of upper states. In all our calculations so far, we relied on the **D**-matrices to tell us what kind of intersections is encountered.

In our recent study of $H_2C_2^+$, varying the hydrogen distances, q_1 and q_2, indicate different types of intersections, which were exposed just by calculating the corresponding **D**-matrices.[2(a)] In the present case of H_2CN, this type of calculation is not satisfying because unit **D**-matrices are not informative enough as contours which miss the topological intersections will also yield unit **D**-matrices. In other words, RT intersections and nontopological intersections both yield unit **D**-matrices. However, the tristate topological (Berry) phases α_{12} for the two situations are different: in the first case this phase equals 2π and in the second zero. Consequently, we calculated the corresponding three-state Berry phases to find out if they are always 2π or for some situations they switch to become, e.g., zero. According to Figs. 5–10 and the results in Table I, we notice that these phases are consistently $\sim 2\pi$, thus the RT parabolic intersections are maintained for all combinations of q_N and q_C presented in this article. It is expected that the larger are the collinear molecules, the situation may become gradually more complicated because of numerous possible partial groupings of atoms.

ACKNOWLEDGMENTS

A.D. acknowledges CSIR, India, for a junior research fellowship. D.M. acknowledges CRNN [conv/002/NanoRAC(2008)], University of Calcutta, and S.A. acknowl-

edges DST, India, for grants in computational facilities. One of us (M.B.) thanks Professor R. Englman for valuable discussions.

[1] G. J. Halász, Á. Vibók, R. Baer, and M. Baer, J. Chem. Phys. **125**, 094102 (2006).
[2] (a) G. J. Halász, Á. Vibók, D. K. Hoffman, D. J. Kouri, and M. Baer, J. Chem. Phys. **126**, 154309 (2007); (b) G. J. Halász, Á. Vibók, R. Baer, and M. Baer, J. Phys. A: Math. Theor. **40**, F267 (2007).
[3] E. Renner, Z. Phys. **92**, 172 (1934).
[4] *Molecular Spectra and Molecular Structure*, edited by G. Herzberg (Krieger, Malabar, 1991), Vol. III.
[5] M. Perić and S. Peyerimhoff, Adv. Chem. Phys. **124**, 583 (2002); M. Peric, R. J. Buenker, and S. Peyerimhoff, Mol. Phys. **59**, 1283 (1986).
[6] Ch. Jungen and A. J. Merer, Mol. Phys. **40**, 1 (1980); **40**, 95 (1980); Ch. Jungen and A. J. Merer, in *Molecular Spectroscopy: Modern Research*, edited by K. N. Rao (Academic, New York, 1977), Vol. 2, p. 127.
[7] R. Barrow, R. N. Dixon, and G. Duxbury, Mol. Phys. **27**, 1217 (1974); A. Alijah and G. Duxbury, *ibid.* **70**, 605 (1990); G. Duxbury, B. McDonald, M. Van Gogh, A. Alijah, Ch. Jungen, and H. Palivan, J. Chem. Phys. **108**, 2336 (1998).
[8] J. M. Brown and F. Jorgenson, Adv. Chem. Phys. **52**, 117 (1983).
[9] M. Baer, *Beyond Born Oppenheimer: Electronic Non-Adiabatic Coupling Terms and Conical Intersections* (Wiley, Hoboken, NJ, 2006), Chaps. 4 and 5.
[10] *The Role of Degenerate States in Chemistry*, Advances in Chemical Physics Vol. 124, edited by M. Baer and G. D. Billing (Wiley-Interscience, Hoboken, NJ, 2002); [in particular, see (a) M. S. Child (pp. 1); (b) S. Adhikari and G. D. Billing (pp. 143); (c) R. Englman and A. Yahalom (pp. 197); (d) A. Kuppermann and R. Abrol (pp. 283); and (e) G. A. Worth and M. A. Robb (pp. 355)].
[11] H. A. Jahn and E. Teller, Proc. R. Soc. London, Ser. A **161**, 220 (1937); M. S. Child and H. C. Longuet Higgins, Philos. Trans. R. Soc. London, Ser. A **254**, 259 (1961); G. Herzberg and H. C. Longuet-Higgins, Discuss. Faraday Soc. **35**, 77 (1963); H. C. Longuet-Higgins, Proc. R. Soc. London, Ser. A **344**, 147 (1975).
[12] R. Englman, *The Jahn-Teller Effect in Molecules and Crystals* (Wiley Interscience, New York, 1972).
[13] C. A. Mead, J. Chem. Phys. **78**, 807 (1983); T. C. Thompson, D. G. Truhlar, and C. A. Mead, *ibid.* **82**, 2392 (1985); Z.-R. Xu, M. Baer, and A. J. C. Varandas, *ibid.* **112**, 2746 (2000); G. J. Halász, Á. Vibók, A. M. Mebel, and M. Baer, *ibid.* **118**, 3052 (2003); S. Han and D. Yarkony, *ibid.* **119**, 5058 (2003).
[14] A. M. Mebel, A. Yahalom, R. Englman, and M. Baer, J. Chem. Phys. **115**, 3673 (2001); T. Vértesi and E. Bene, Chem. Phys. Lett. **392**, 17 (2004); S. Al-Jabour, M. Baer, O. Deeb, M. Liebscher, J. Manz, X. Xu, and S. Zilberg, J. Phys. Chem. A **114**, 2991 (2010).
[15] T. Vértesi and R. Englman, J. Phys. B **41**, 025102 (2008).
[16] G. J. Halász and Á. Vibók (private communication).
[17] MOLPRO, a package of *ab initio* programs designed by H.-J. Werner and P. J. Knowles with contributions from J. Almlöf, R. Amos, S. Elbert, C. Hampel, W. Meyer, K. Peterson, R. Pitzer, and A. Stone.
[18] M. Born and J. R. Oppenheimer, Ann. Phys. **84**, 457 (1927); M. Born, Festschrift Göttingen Nach. Math. Phys. **K1**, 1 (1951); M. Born and K. Huang, *Dynamical Theory of Crystal Lattices* (Oxford University, New York, 1954), Chap. IV.
[19] (a) M. Baer, Chem. Phys. Lett. **35**, 112 (1975); (b) (Ref. 9), Sec. 4.2; (c) (Ref. 9), Sec. 1.2.
[20] (a) M. Baer, Mol. Phys. **40**, 1011 (1980); (b) (Ref. 9), Chap. 1; (c) I. Ryb and R. Baer, J. Chem. Phys. **121**, 10370 (2004); (d) R. Baer, *ibid.* **117**, 7405 (2002).
[21] (a) M. Baer and A. Alijah, Chem. Phys. Lett. **319**, 489 (2000); (b) M. Baer, S. H. Lin, A. Alijah, S. Adhikari, and G. D. Billing, Phys. Rev. A **62**, 032506 (2000); (c) (Ref. 9), Sec. 2.1.3.3; (d) J. Avery, M. Baer, and G. D. Billing, Mol. Phys. **100**, 1011 (2002).
[22] (a) Z. H. Top and M. Baer, J. Chem. Phys. **66**, 1363 (1977); (b) A. Alijah and M. Baer, J. Phys. Chem. A **104**, 389 (2000); (c) T. Vértesi, E. Bene, A. Vibok, G. J. Halasz, and M. Baer, *ibid.* **109**, 3476 (2005); (d) B. Sarkar and S. Adhikari, J. Chem. Phys. **124**, 074101 (2006); (e) (Ref. 9), Sec. 8.3.3.2.
[23] M. S. Kaczmarski, Y. Ma, and M. Rohlfing, Phys. Rev. B **81**, 115433 (2010); M. S. Kaczmarski and M. Rohlfing, J. Phys. B **43**, 051001 (2010); P. O. Godsi, C. R. Evenhuis, and M. A. Collins, J. Chem. Phys. **125**, 104105 (2006); A. Kuppermann and R. Abrol, Adv. Chem. Phys. **124**, 323 (2002).
[24] (a) M. V. Berry, Proc. R. Soc. London, Ser. A **392**, 45 (1984); (b) M. Baer and R. Englman, Mol. Phys. **75**, 293 (1992).
[25] M. Baer, T. Vertesi, G. J. Halasz, A. Vibok, and S. Suhai, Faraday Discuss. **127**, 337 (2004); D. R. Yarkony, J. Chem. Phys. **105**, 10456 (1996); P. Barragan, L. F. Errea, A. Macias, L. Mendez, A. Riera, J. M. Lucas, and A. Aguilar, *ibid.* **121**, 11629 (2004); C. Hu, H. Hirai, and O. Sugino, *ibid.* **128**, 144111 (2008); **127**, 064103 (2007); R. Baer, Phys. Rev. Lett. **104**, 073001 (2010).